

Constraining theoretical Corrections to Gamow-Teller Transition Rates

L. Xayavong^{1,*} and Y. Lim^{1,†}

¹*Department of Physics, Yonsei University, Seoul 03722, South Korea*

(Dated: February 5, 2024)

We propose two novel constraints for the theoretical corrections to Gamow-Teller transition rates. The first, derived from a two-level model, predicts forbidden regions within the plane defined by the isospin-mixing correction, δ_{C1} , and the ratio, η , of the isospin-symmetry Gamow-Teller matrix elements between the upper and lower admixed states. It serves as a filter for the theoretical calculations, particularly effective for small values of $|\eta|$. The other employs experimental ft values, incorporating the upper admixed states, and exploits mirror symmetry to eliminate isospin-invariant and nuclear structure-independent quantities. This approach not only offers an alternative mean for collectively testing theoretical corrections but also, as a byproduct, enables the extraction of η^2 . This provides another sensitive test for the isospin-conserving component of nuclear Hamiltonian. Our investigation reveals a substantial cancellation of among radiative correction contributions in these tests.

Introduction : In the standard-model framework, the Gamow-Teller (GT) process is governed by the axial-vector term of the weak current. In the non-relativistic limit, this term reduces to the operator $\sigma\tau_{\pm}$, allowing for a change of total angular momentum and isospin by one unit. Consequently, acting this operator on a specific initial state can result in several possible final states. Due to this characteristic, the theoretical description of GT transitions strongly depends on the chosen model of nuclear structure [1–7]. Notably, unlike the Fermi matrix elements which are solely determined by the isospin quantum numbers, the GT matrix elements, even between states with definite isospin, are not analytically known. Understanding the impact of isospin-symmetry breaking on this process poses an even greater challenge, since isospin-nonconserving interactions constitute only a small portion of the complete nuclear Hamiltonian [8–14].

The master formula for GT transitions is expressed as

$$ft(1 + \delta'_R)(1 - \delta_C + \delta_{NS}) = \frac{K}{\mathcal{M}^2 G_F^2 q_A^2 g_A^2 V_{ud}^2 (1 + \Delta_R)}, \quad (1)$$

where the left-hand side contains the experimental ft value, which is the product of the statistical rate function (f) and partial half-life (t), along with theoretical corrections δ_C , δ'_R , and δ_{NS} . These corrections account for isospin-symmetry breaking, transition-dependent, and nuclear structure-dependent radiative effects, respectively. On the right-hand side, apart from the isospin-symmetry GT matrix element, \mathcal{M} and its quenching factor q_A that compensates for the systematic deviation of shell-model predictions from experimentally deduced values [1, 2], only nucleus-independent quantities are present. These include K , a combination of fundamental constants [15]; G_F and g_A , the Fermi [16, 17] and axial-vector coupling [18, 19] constants, respectively; Δ_R , another radiative correction term that merely depends on a specific type of weak current [20–22]; and V_{ud} , the top-left element of the Cabibbo–Kobayashi–Maskawa

quark-mixing matrix [15, 23, 24]. When considering a pair of mirror GT transitions, all universal constants and isospin-invariant quantities in Eq. (1) can be eliminated. The obtained equation at first order is,

$$\Delta_I \approx \frac{ft^+}{ft^-} - (\delta_C^+ - \delta_C^-) + (\delta_{NS}^+ - \delta_{NS}^-) + (\delta_R^+ - \delta_R^-) - 1, \quad (2)$$

where the label ‘+’ (‘-’) correspond to the β^+ (β^-) emission. Given the expectation of a zero residual ($\Delta_I = 0$), Eq. (2) has been used as a collective test for theoretical corrections on its right-hand side, employing the experimental data on ft^+/ft^- . A notable agreement was achieved between theoretical predictions and experimental data in the previous shell-model studies [9, 14], although $(\delta_{NS}^+ - \delta_{NS}^-) = 0$ and $(\delta_R^+ - \delta_R^-) = 0$ were assumed. In general, both of these radiative corrections consist of a small isovector component [25, 26] that could contribute to a mirror asymmetry. A finite value of Δ_I could also be attributed to the existence of second-class weak currents [27–30], which are absent in the standard model. Δ_I beyond standard model, however, seems to be negligible compared to current uncertainties in nuclear structure calculations [14, 15, 31, 32]. Within the shell-model framework, δ_C can be decomposed into two components:

$$\delta_C \approx \delta_{C1} + \delta_{C2}, \quad (3)$$

where δ_{C1} accounts for configuration admixtures within the shell-model valence space induced by the isospin-nonconserving part of the effective Hamiltonian. Whereas, δ_{C2} accounts for the mismatch between proton and neutron radial wave functions, compensating for the isospin admixtures extending beyond the shell-model valence space. The interference terms are of higher orders. For additional details, please refer to Refs. [13, 14].

The purpose of this Letter is to introduce two novel constraints for theoretical corrections, offering a greater selectivity compared to Eq. (2). One of them is exclusively sensitive to δ_{C1} and relies only on predictions

of a two-level model of isospin mixing[14], without the need for experimental data. This method can be expected to work at the weak isospin-mixing limit. The other, although originated from the master formula (1), differs from Eq. (2) by incorporating GT transitions to second admixed states. This introduces a novel collective test for theoretical corrections. Additionally, the contributions of the radiative corrections are empirically investigated based on the existing results obtained for superallowed $0^+ \rightarrow 0^+$ Fermi β decay [25, 26]. It is also demonstrated that the inclusion of an upper pair of mirror GT transitions allows for an experimental determination of η^2 , serving as a test, which is solely dependent on the isospin-symmetry part of the nuclear Hamiltonian.

Formalism: While an exact shell-model calculation of δ_{C1} for a GT transition is extremely complicated, certain fundamental properties of this correction term can be identified using a fully analytic two-level mixing model [14]. Specifically, it describes δ_{C1} as a function of the isospin-mixing amplitude, α , namely

$$\delta_{C1} = -2\eta\alpha + (1 - \eta^2)\alpha^2 + \mathcal{O}(\alpha^3), \quad (4)$$

where $\eta = \mathcal{M}_1/\mathcal{M}_0$, representing the ratio of the isospin-symmetry GT matrix elements between the upper (labeled as 1) and the lower (labeled as 0) admixed states. Note that the standard definition of δ_{C1} , namely $\delta_{C1} = 1 - (M/\mathcal{M}_0)^2$ where M denotes the exact GT matrix element for the lower admixed state¹, is utilized in deriving Eq. (4). For simplicity, we also assume that $|\alpha|$ is sufficiently small to make the terms beyond the second order in Eq. (4) negligible. According to first-order perturbation theory, α is inversely proportional to the energy separation between admixed states. Consequently, couplings of the lowest state with those above the second state diminish progressively, justifying the use of the two-level mixing model. While it is also possible to derive a similar δ_{C1} formula for the upper admixed state (the second state), the justification for the two-level mixing might not hold due to its significant coupling to the next excited state². Hence, our study based on this simplified model exclusively concentrates on δ_{C1} for GT transitions to the lowest state. It is important to emphasize that Eq. (4) predicts essential characteristics of δ_{C1} specific to

GT transitions. One of these is that δ_{C1} can be positive or negative, depending on both sign and magnitude of α and η . A negative δ_{C1} results in increases in $|M|$ due to the dominant constructive contribution from the upper admixed state. Conversely, a positive δ_{C1} produces the opposite effect. Another interesting observation arises when $\eta = 0$, as in cases where the isospin quantum number of the upper admixed state differs from that of the initial state by more than one unit. In this situation, we obtain $\delta_{C1} = \alpha^2$, akin to what is observed in Fermi transitions [33]. In addition, the presence of the first-order term in α in Eq. (4) implies that α must be a real number. Roots of the quadratic equation (4) take the forms,

$$\alpha = \kappa \left(1 \pm \sqrt{1 + \frac{\delta_{C1}}{\eta\kappa}} \right), \quad (5)$$

where $\kappa = \eta/(1 - \eta^2)$. The requirement of $\Im(\alpha) = 0$ implies that the expression inside the square root in Eq. (5) must be positive, leading to the following boundaries,

$$-\frac{\eta^2}{1 - \eta^2} \leq \delta_{C1} \leq 1, \quad \text{if } |\eta| < 1. \quad (6)$$

The sign in front of the square root in Eq. (5) can be fixed by applying $0 \leq \alpha^2 \leq 1$, as α represents a probability amplitude. Taking the square to Eq. (5) yields,

$$\alpha^2 = \kappa^2 \left[2 + \frac{\delta_{C1}}{\eta\kappa} \pm \left(2 + \frac{\delta_{C1}}{\eta\kappa} - \frac{\delta_{C1}^2}{4\eta^2\kappa^2} \right) \right] + \mathcal{O}(\delta_{C1}^3). \quad (7)$$

It can be shown that the positive sign imposes restrictions on certain values of η without theoretical justification. Therefore, it is disregarded. The negative sign results in the following boundaries, definite for all η values,

$$-2\eta \leq \delta_{C1} \leq 2\eta. \quad (8)$$

Note also that $\delta_{C1} \leq 1$ holds by definition, irrespective of η . The combination of Eqs. (6) and (8) results in,

$$\begin{cases} -\frac{\eta^2}{1 - \eta^2} \leq \delta_{C1} \leq 2\eta, & \text{if } |\eta| < \frac{1}{2} \\ -\frac{\eta^2}{1 - \eta^2} \leq \delta_{C1} \leq 1, & \text{if } \frac{1}{2} \leq |\eta| < \frac{1}{4}(\sqrt{17} - 1) \\ -2\eta \leq \delta_{C1} \leq 1, & \text{otherwise.} \end{cases} \quad (9)$$

It should be noticed that Eq.(9) yields δ_{C1} equals 0 at $\eta = 0$. This conflicts with the expectation from Eq.(4), the starting point of our analysis, where we determine $\delta_{C1} = \alpha^2$ for $\eta = 0$, as in Fermi transitions. Hence, it is logical to state that the error in Eq.(9) is, at least, of order $\mathcal{O}(\alpha^2)$. A finer precision might be available if the higher-order terms are included in the Taylor expansion (7). The physically admissible regions in the (η, δ_{C1}) plane defined by Eq. (9), are represented as the shaded areas in Fig. 1.

¹ In the two-level mixing model, this matrix element can be expressed as $M = \sqrt{1 - \alpha^2}\mathcal{M}_0 + \alpha\mathcal{M}_1$.

² In general, the density of states increases with excitation energy. Therefore, the energy separation between the first and second states is generally larger than that between the second and third states.

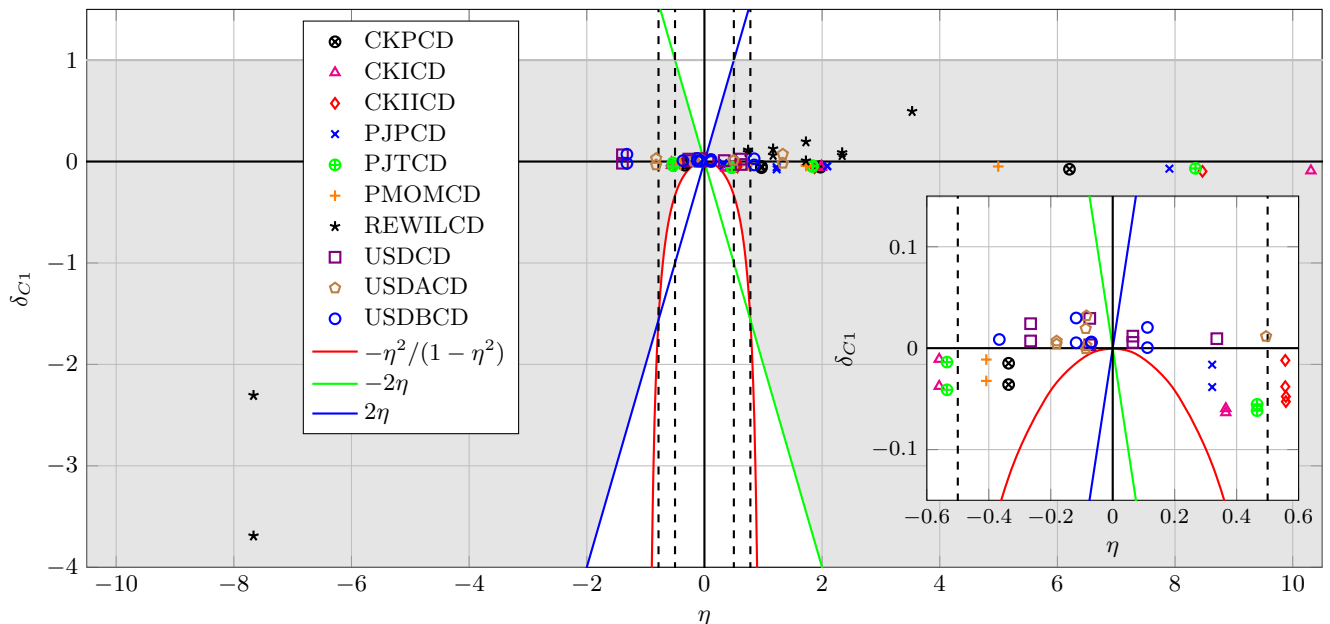


FIG. 1. The shaded areas illustrate the physical admissible regions of δ_{C1} based on the predictions from the two-level model. The points represent shell-model values obtained with various effective interactions, mainly taken from Ref. [14]. Additionally, data for GT transitions to excited states, not covered in Ref. [14], are calculated with the same model spaces and effective Hamiltonian.

To demonstrate the applicability of the boundaries (9) as a means for testing theoretical calculations of δ_{C1} , we incorporate the shell-model results for the sixteen pairs of mirror GT transitions in the p and sd shells given in Ref. [14] into Fig. 1. Additional data for GT transitions to excited states, not considered in Ref. [14] have been calculated within a similar approach. These theoretical data were obtained using exact diagonalizations of well-established effective isospin-nonconserving Hamiltonians and their corresponding isospin-symmetry versions for a selected model space. It is seen from Fig. 1 that all the shell-model values are located inside the admissible regions, even under extreme scenarios where the two-level mixing model is not expected to be valid. Notably, the two large negative values near the bottom-left corner of the graph correspond to the decays of $^{22}\text{O}(\beta^-)^{22}\text{F}$ and $^{22}\text{Si}(\beta^+)^{22}\text{Al}$, where an exceptionally strong isospin mixing has been experimentally observed [35]. This test is particularly precise when η has a small magnitude, narrowing admissible regions.

To establish a new experimental constraint, we compare the master formula, Eq. (1), between GT transitions to the first and second admixed states. In this way, all nuclear structure-independent quantities on the right-hand side of Eq. (1) can be eliminated. The resulting expres-

sion reads

$$\Delta_{II} \approx \eta^2 - \frac{ft^0}{ft^1} [1 + (\delta_R^0 - \delta_R^1) + (\delta_{NS}^0 - \delta_{NS}^1) - (\delta_C^0 - \delta_C^1)]. \quad (10)$$

It is observed that Eq. (10) is analogous to Eq. (2); they differ only by the interchange of the labels 0(1) with +(-) and the presence of η in the former, which arises from the lack of analogy between lower and upper admixed states. In principle, ‘0’ and ‘1’ could be any pair of excited states, given the availability of their corresponding ft values. Since $\Delta_{II} = 0$ is expected, Eq. (10) serves as an alternative collective test for the theoretical corrections, including δ_R^0 , δ_R^1 , δ_{NS}^0 , δ_{NS}^1 , δ_C^0 and δ_C^1 , together with η^2 , using experimental data on ft^0/ft^1 . The requirement of $\Im(\eta) = 0$ also implies an additional constraint among these theoretical corrections:

$$(\delta_C^0 - \delta_C^1) \leq 1 + (\delta_R^0 - \delta_R^1) + (\delta_{NS}^0 - \delta_{NS}^1). \quad (11)$$

With $(\delta_R^0 - \delta_R^1) + (\delta_{NS}^0 - \delta_{NS}^1) = 0$, our shell-model results meet the condition (11) except for $^{21}\text{F}(\beta^-)^{21}\text{Ne}$ and $^{21}\text{Mg}(\beta^+)^{21}\text{Na}$, decaying to the second $\frac{5}{2}^+$ states. Our calculation for this exceptional case yields $\mathcal{M}_1 \approx 0$ which leads to a divergence in δ_C^3 . These transitions are thus

³ The leading terms of the correction are inversely proportional to the isospin-symmetry GT matrix element. See, for example, Ref. [14]

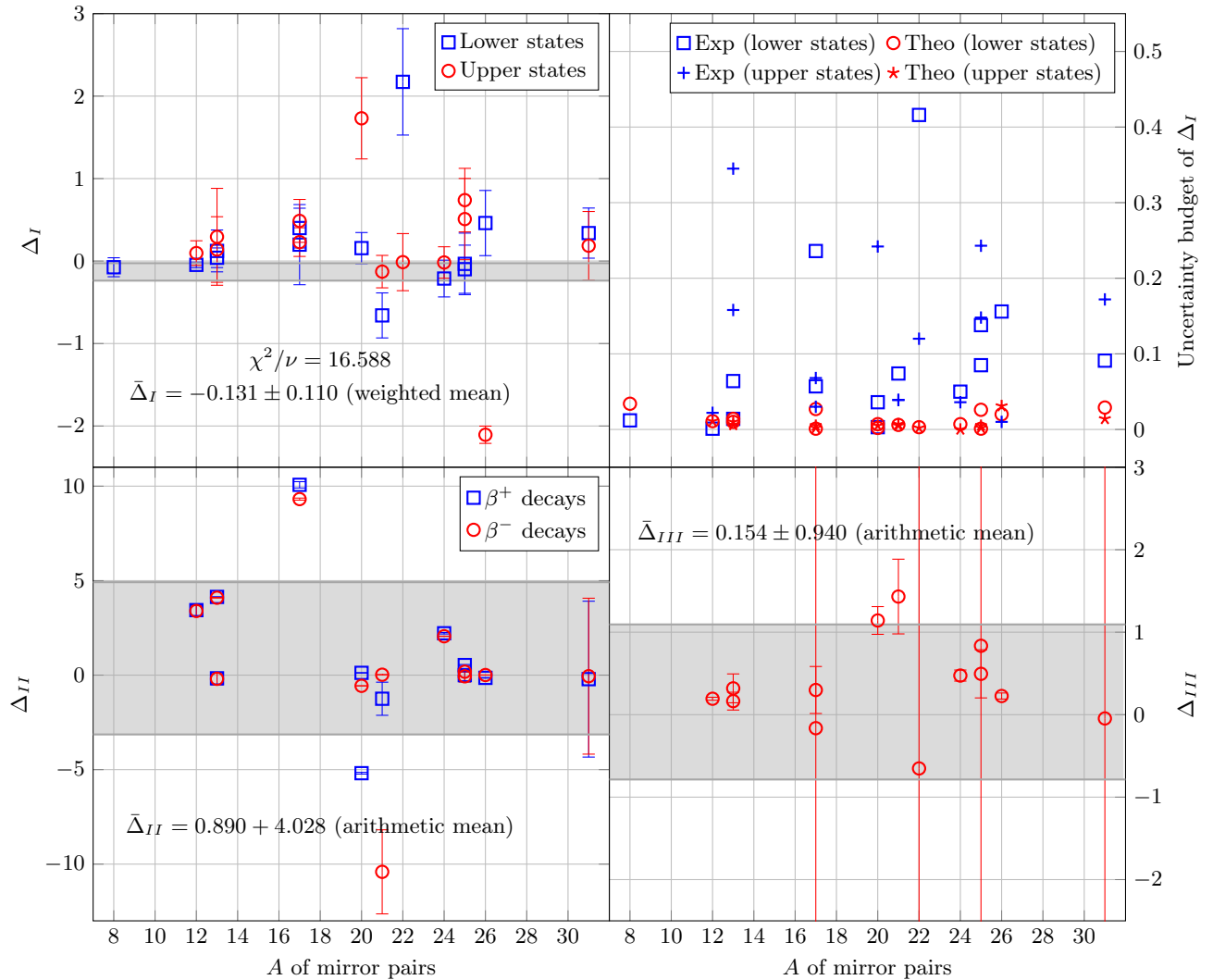


FIG. 2. (Color online) Illustration of the shell-model tests for the residuals defined in Eq. (2), (10), and (12). The gray bands indicate the averages. The top-right panel displays the individual contributions to uncertainties of Δ_I . The experimental inputs (ft values) are taken from Ref. [34].

excluded in the following studies. Among the remaining transitions, the largest ($\delta_C^0 - \delta_C^1$) values are approximately 55% corresponding to the decays of $^{17}\text{Ne}(\beta^+)^{17}\text{F}$ and $^{26}\text{Na}(\beta^-)^{26}\text{Mg}$. Furthermore, Eq. (10) enables the extraction of η^2 when the contribution from the corrective terms on its right-hand side are insignificant. Essentially, η^2 solely depends on the isospin-symmetry component of the nuclear Hamiltonian. The comparison between these experimentally extracted and shell-model values of η^2 is given in Table I. While both datasets are found to be consistent with the boundaries (9) and the shell-model values for δ_{C1} , a substantial discrepancy emerges between them in the majority of cases.

According to previous studies on the superallowed $0^+ \rightarrow 0^+$ Fermi β decay [25, 33], δ'_R comprises two components: one dependent on the atomic number, Z and the other on the transition Q value. The Z -dependent

component is common for both transitions to lower and upper admixed states, thus not contributing to Δ_{II} . Additionally, the universal Born-graph contribution to δ_{NS} should cancel out identically in Eq. (10). This latter cancellation also applies to Δ_I in Eq. (2). It is clearly seen from Table I that, despite allowing for a conservative 50% uncertainty to cover the remaining contribution of the missing radiative corrections, significant discrepancies between the experimental η^2 values and the shell-model predictions persist. Therefore, it is likely that η^2 is the largest uncertainty source in Eq. (10). In order to eliminate this isospin-invariant parameter from Eq. (10), we combine two pairs of mirror GT transitions, leading

TABLE I. Comparison of η^2 between the values extracted from experimental ft^0/ft^1 data via Eq. (10) neglecting the theoretical corrections, and those obtained from shell-model calculations. The experimental η^2 values are averaged between β^+ transitions and their β^- mirror partners. Columns five and six list the shell-model values for $\delta_C^0 - \delta_C^1$, expressed as percentages, which are to be validated with Eq.(11).

Mirror pairs	$J_i^\pi T_i$	$J_f^\pi T_f$ ^d	η_{exp}^2	η_{theo}^2	$\delta_C^0 - \delta_C^1$ (β^+)	$\delta_C^0 - \delta_C^1$ (β^-)
${}^8\text{Li}(\beta^-){}^8\text{Be}; {}^8\text{B}(\beta^+){}^8\text{Be}$	2^+1	2^+0	409.261 ± 20.723	56.454 ± 27.235^a	0.674 ± 2.622	-12.556 ± 3.194
${}^{12}\text{B}(\beta^-){}^{12}\text{C}; {}^{12}\text{N}(\beta^+){}^{12}\text{C}$	1^+1	0^+0	0.308 ± 0.004	3.722 ± 0.285^a	8.413 ± 1.234	-5.545 ± 0.901
${}^{13}\text{B}(\beta^-){}^{13}\text{C}; {}^{13}\text{O}(\beta^+){}^{13}\text{N}$	$\frac{3}{2}^- \frac{3}{2}$	$\frac{1}{2}^- \frac{1}{2}$	0.271 ± 0.026	0.110 ± 0.320	-5.396 ± 0.419	-9.409 ± 1.044
	$\frac{3}{2}^- \frac{3}{2}$	$\frac{3}{2}^- \frac{1}{2}$	0.302 ± 0.054	4.419 ± 0.400^a	2.820 ± 1.522	-2.158 ± 0.659
${}^{17}\text{N}(\beta^-){}^{17}\text{O}; {}^{17}\text{Ne}(\beta^+){}^{17}\text{F}$	$\frac{1}{2}^- \frac{3}{2}$	$\frac{3}{2}^- \frac{1}{2}$	4.626 ± 0.139	12.460^a	57.994 ± 2.633	14.344 ± 0.694
	$\frac{1}{2}^- \frac{3}{2}$	$\frac{1}{2}^- \frac{1}{2}$	444.048 ± 62.749	12.429^a	-2.259 ± 0.160	8.124 ± 0.117
${}^{20}\text{F}(\beta^-){}^{20}\text{Ne}; {}^{20}\text{Na}(\beta^+){}^{20}\text{Ne}$	2^+1	2^+0	6.180 ± 0.047	1.361^a	-5.963 ± 0.682	-14.205 ± 0.248
${}^{20}\text{O}(\beta^-){}^{20}\text{F}; {}^{20}\text{Mg}(\beta^+){}^{20}\text{Na}$	0^+2	1^+1	0.869 ± 0.058	0.551	23.498 ± 0.532	10.011 ± 0.138
${}^{21}\text{F}(\beta^-){}^{21}\text{Ne}; {}^{21}\text{Mg}(\beta^+){}^{21}\text{Na}$	$\frac{5}{2}^+ \frac{3}{2}$	$\frac{3}{2}^+ \frac{1}{2}$	9.651 ± 1.345	5.479	-11.661 ± 0.736	-12.463 ± 0.239
	$\frac{5}{2}^+ \frac{3}{2}$	$\frac{5}{2}^+ \frac{1}{2}$	16.764 ± 5.383	0.017^a	428.109 ± 0.654^b	262.784 ± 0.350^b
${}^{22}\text{O}(\beta^-){}^{22}\text{F}; {}^{22}\text{Si}(\beta^+){}^{22}\text{Al}$	0^+3	1^+2	11.484 ± 1.346	58.757^a	0.922 ± 0.144	17.693 ± 0.324
${}^{24}\text{Ne}(\beta^-){}^{24}\text{Na}; {}^{24}\text{Si}(\beta^+){}^{24}\text{Al}$	0^+2	1^+1	0.866 ± 0.030	2.976^a	6.471 ± 0.498	0.098 ± 0.428
${}^{25}\text{Na}(\beta^-){}^{25}\text{Mg}; {}^{25}\text{Si}(\beta^+){}^{25}\text{Al}$	$\frac{5}{2}^+ \frac{3}{2}$	$\frac{5}{2}^+ \frac{1}{2}$	0.133 ± 0.019	0.111 ± 0.307	-3.560 ± 2.541	-7.652 ± 0.835
	$\frac{5}{2}^+ \frac{3}{2}$	$\frac{3}{2}^+ \frac{1}{2}$	0.560 ± 0.048	0.913 ± 0.355	9.096 ± 0.223	-0.919 ± 0.017
${}^{26}\text{Na}(\beta^-){}^{26}\text{Mg}; {}^{26}\text{P}(\beta^+){}^{26}\text{Si}$	3^+2	2^+1	0.031 ± 0.010	0.006 ± 0.004	-48.954 ± 3.456	54.833 ± 1.196
${}^{31}\text{Al}(\beta^-){}^{31}\text{Si}; {}^{31}\text{Ar}(\beta^+){}^{31}\text{Cl}$	$\frac{5}{2}^+ \frac{5}{2}$	$\frac{3}{2}^+ \frac{3}{2}$	2.192 ± 0.222	1.785 ± 4.123	16.739 ± 2.965	7.789 ± 1.273

^a Disagree within conservative 50 % experimental error.

^b According to Eq. (11), these values, exceeding 100%, would be unphysical if $(\delta_R^0 - \delta_R^1) + (\delta_{NS}^0 - \delta_{NS}^1) \approx 0$.

^c The isospin quantum numbers for the first and second admixed states are identical for all cases.

to

$$\begin{aligned}
\Delta_{III} \approx & \frac{ft^{0-} ft^{1+}}{ft^{0+} ft^{1-}} - (\delta_R^{0+} - \delta_R^{0-}) + (\delta_R^{1+} - \delta_R^{1-}) \\
& - (\delta_{NS}^{0+} - \delta_{NS}^{0-}) + (\delta_{NS}^{1+} - \delta_{NS}^{1-}) + (\delta_C^{0+} - \delta_C^{0-}) \\
& + (\delta_C^{1+} - \delta_C^{1-}) - 1.
\end{aligned} \tag{12}$$

Again, the residual Δ_{III} should vanish when appropriate theoretical and experimental inputs are provided. As an interesting feature of Eq. (12), any Z - and Q -dependent components embedded in the theoretical corrections would be almost completely canceled out, due to the double subtraction. Therefore, the term $(\delta_R^{1+} - \delta_R^{1-}) - (\delta_R^{0+} - \delta_R^{0-})$ is expected to vanish. Regarding δ_{NS} , besides the previously mentioned universal Born-graph contribution, it comprises an orbital isoscalar, spin isoscalar, orbital isovector, and spin isovector components [25, 36]. Both isoscalar components do not contribute to Δ_I and Δ_{III} . However, the isovector components exhibit a sign reversal under the mirror symmetry, while maintaining a consistent magnitude. Consequently, the isovector contribution to Δ_{III} could be significant similar to Δ_I , or negligible if substantial cancellation occurs between the lower and upper admixed states. A further detailed study of these radiative corrections would be highly necessary.

We have investigated the residual Δ_I , Δ_{II} and Δ_{III} using the experimental ft values from Ref. [34] and our shell-model results [14]. Apart from the previously men-

tioned calculations of δ_{C1} , the other leading-order term, δ_{C2} , is evaluated with realistic Woods-Saxon radial wave functions. The potential depth and length parameter are readjusted to reproduce separation energies and charge radii whenever data are available. The uncertainty on δ_{C1} reflects the spread among different effective isospin-nonconserving interactions considered in the calculations. Meanwhile, the uncertainty on δ_{C2} arises from the variation due to different fitting methods and experimental errors in available charge-radius data. Further details on our uncertainty quantification can be found in Refs. [11, 14]. The radiative corrections, δ'_R and δ_{NS} are not included due to the lack of numerical data.

Our results of experimental tests for the thirty-two pairs of mirror GT transitions, including upper admixed states, are illustrated in Fig. 2. The obtained Δ_I values are displayed in the top-left panel, and their individual uncertainty contributions in the top-right panel. The values of Δ_{II} and Δ_{III} are shown in the bottom-left and bottom-right panels, respectively. Among these three experimental tests, it is evident that Δ_I exhibits the greatest consistency. The corresponding χ^2/ν value is 16.588. This large χ^2/ν indicates a potential underestimate of the overall uncertainty and, possibly, the significance of the absent radiative corrections. Nevertheless, its weighted average is reasonably close to the ideal value, namely $\Delta_I = -0.131 \pm 0.110$. As indicated in the uncertainty budget provided in the top-right panel of Fig. 2, experimental errors predominantly dominate in most cases. In

particular, we assume a zero uncertainty on δ_{C1} for nuclei resided in the $p - sd$ cross-shell region, due to the availability of only a single effective isospin-nonconserving interaction. Unexpectedly, the resulting values for the residual Δ_{II} deviate substantially from zero, with deviations largely exceeding the overall uncertainty, except for a few cases. Furthermore, the consistency of the Δ_{II} values cannot be maintained even if a conservative 100 % uncertainty is assumed for the isospin-symmetry breaking corrections. This strongly suggests the significance of the missing radiative corrections or, more likely, the unreliability of the shell-model values of η^2 . The arithmetic mean of Δ_{II} is 0.890 ± 4.028 . However, it is interesting to remark that the Δ_{II} values for a given pair of mirror GT transitions are nearly coincident. This observation seems to indicate that the missing radiative corrections are nearly invariant under the mirror symmetry as expected, despite the significance of their individual values.

The last experimental test of our theoretical calculations is based on the residual Δ_{III} . From the results displayed in the bottom-right panel of Fig. 2, Δ_{III} values are much closer to zero compared with those of Δ_{II} , due to the mirror symmetry property of the missing radiative corrections, as remarked above. Nevertheless, it is likely that the overall uncertainties of Δ_{III} are underestimated for most cases, except for $A = 17, 22, 25$ and 31. Excluding these exceptional cases, this test yields an extremely large χ^2/ν value. The arithmetic mean of Δ_{III} is 0.154 ± 0.940 .

Conclusion: To summarize, the boundaries (9), derived from the simplified two-level isospin-mixing model, define permissible regions in the (η, δ_{C1}) plane. This serves as a filter for theoretical calculations, particularly when η approaches zero. Our current shell-model results successfully satisfy this criterion for all transitions, including $A = 22$ where an exceptionally strong isospin mixing has been observed. Regarding the experimental tests, the remaining deviations of Δ_I and Δ_{III} from zero seems to be principally due to inaccuracy in our theoretical calculations of the isospin-symmetry breaking correction and errors in the experimental data. The contributions of the radiative corrections to these residuals are expected to be negligible owing to the mirror symmetry, especially for Δ_{III} . Conversely, Δ_{II} is substantially deteriorated as the result of the unreliability of the shell-model prediction of η^2 , and possibly the absence of the radiative corrections. As a byproduct, the incorporation of the upper admixed states enable the experimental extraction of η^2 . This serves as a test exclusively sensitive to the isospin-symmetry part of the nuclear Hamiltonian. Remarkably, this test was found to be meaningful in several cases, even if a conservative 50 % uncertainty is assumed to cover the corrective contributions.

L. Xayavong and Y. Lim are supported by the National Research Foundation of Korea(NRF) grant funded by

the Korea government(MSIT)(No. 2021R1A2C2094378). Y. Lim is also supported by the Yonsei University Research Fund of 2023-22-0126.

* xayavong.latsamy@yonsei.ac.kr

† ylim@yonsei.ac.kr

- [1] P. Gysbers *et al.*, Nat. Phys. **15**, 428 (2019).
- [2] B. Brown and B. Wildenthal, Atomic Data and Nuclear Data Tables **33**, 347 (1985).
- [3] V. Kumar and P. C. Srivastava, Eur. Phys. J. A. **52**, 181 (2016).
- [4] E. M. Ney, J. Engel, and N. Schunck, Phys. Rev. C **105**, 034349 (2022).
- [5] D. Wilkinson, Nucl. Phys. A **225**, 365 (1974).
- [6] D. H. Wilkinson, Phys. Rev. C **7**, 930 (1973).
- [7] D. Wilkinson, Nucl. Phys. A **209**, 470 (1973).
- [8] W. Ormand and B. Brown, Nucl. Phys. A **440**, 274 (1985).
- [9] N. Smirnova and C. Volpe, Nucl. Phys. A **714**, 441 (2003).
- [10] Y. H. Lam, N. A. Smirnova, and E. Caurier, Phys. Rev. C **87**, 054304 (2013).
- [11] L. Xayavong and N. A. Smirnova, Phys. Rev. C **97**, 024324 (2018).
- [12] L. Xayavong and N. A. Smirnova, Phys. Rev. C **105**, 044308 (2022).
- [13] L. Xayavong and N. A. Smirnova, Phys. Rev. C **109**, 014317 (2024).
- [14] L. Xayavong and Y. Lim, Shell-model description of the isospin-symmetry-breaking correction to gamow-teller β -decay rates and their mirror asymmetries (2023), arXiv:2312.07900 [nucl-th].
- [15] J. C. Hardy and I. S. Towner, Phys. Rev. C **102**, 045501 (2020).
- [16] D. M. Webber *et al.* (MuLan Collaboration), Phys. Rev. Lett. **106**, 041803 (2011).
- [17] R. Carey, T. Gorringer, and D. Hertzog, SciPost Phys. Proc. , 016 (2021).
- [18] B. Märkisch *et al.*, Phys. Rev. Lett. **122**, 242501 (2019).
- [19] A. F. Leder *et al.*, Phys. Rev. Lett. **129**, 232502 (2022).
- [20] L. Hayen, Phys. Rev. D **103**, 113001 (2021).
- [21] V. Cirigliano *et al.*, Phys. Rev. D **108**, 053003 (2023).
- [22] C.-Y. Seng, M. Gorchtein, and M. J. Ramsey-Musolf, Phys. Rev. D **100**, 013001 (2019).
- [23] N. Cabibbo, Phys. Rev. Lett. **10**, 531 (1963).
- [24] M. Kobayashi and T. Maskawa, Progress of Theoretical Physics **49**, 652 (1973), <https://academic.oup.com/ptp/article-pdf/49/2/652/5257692/49-2-652.pdf>.
- [25] I. S. Towner and J. C. Hardy, Phys. Rev. C **66**, 035501 (2002).
- [26] I. Towner, Nucl. Phys. A **540**, 478 (1992).
- [27] S. Weinberg, Phys. Rev. **112**, 1375 (1958).
- [28] J. N. Huffaker and E. Greuling, Phys. Rev. **132**, 738 (1963).
- [29] J. Delorme and M. Rho, Nucl. Phys. B **34**, 317 (1971).
- [30] D. Wilkinson, Eur. Phys. J. A **7**, 307 (2000).
- [31] A. T. Gallant *et al.*, Phys. Rev. Lett. **130**, 192502 (2023).
- [32] M. T. Burkey *et al.*, Phys. Rev. Lett. **128**, 202502 (2022).
- [33] I. S. Towner and J. C. Hardy, Phys. Rev. C **77**, 025501 (2008).

- (2008).
- [34] National Nuclear Data Center (NNDC), Evaluated nuclear structure data file (ensdf), <https://www.nndc.bnl.gov/ensdf/> (2024).
- [35] J. Lee *et al.* (RIBLL Collaboration), Phys. Rev. Lett. **125**, 192503 (2020).
- [36] I. Towner, Nucl. Phys. A **216**, 589 (1973).

Supplementary material

TABLE II. Numerical results of the shell-model calculations for the ratio η and the total isospin-symmetry breaking correction. The + (-) label indicates the β^+ (β^-) decays. The 0 (1) label indicates the lower (upper) admixed states. The unit of the correction is %.

Mirror pairs	$J_i^\pi T_i$	$J_f^\pi T_f$	η	δ_C^{0-}	δ_C^{0+}	δ_C^{1-}	δ_C^{1+}
${}^8\text{Li}(\beta^-){}^8\text{Be}; {}^8\text{B}(\beta^+){}^8\text{Be}$	2^+1	2^+0	7.514 ± 1.812	-7.924 ± 2.647	7.440 ± 2.074	4.632 ± 1.788	6.766 ± 1.604
${}^{12}\text{B}(\beta^-){}^{12}\text{C}; {}^{12}\text{N}(\beta^+){}^{12}\text{C}$	1^+1	0^+0	1.929 ± 0.074	-4.976 ± 0.636	11.530 ± 0.840	0.569 ± 0.638	3.117 ± 0.904
${}^{13}\text{B}(\beta^-){}^{13}\text{C}; {}^{13}\text{O}(\beta^+){}^{13}\text{N}$	$\frac{3}{2}^-\frac{3}{2}$	$\frac{1}{2}^-\frac{1}{2}$	0.332 ± 0.481	-2.981 ± 0.955	4.484 ± 0.221	6.428 ± 0.421	9.880 ± 0.356
	$\frac{3}{2}^-\frac{3}{2}$	$\frac{3}{2}^-\frac{1}{2}$	2.102 ± 0.000	-8.281 ± 0.278	5.327 ± 1.330	-6.123 ± 0.598	2.507 ± 0.740
${}^{17}\text{N}(\beta^-){}^{17}\text{O}; {}^{17}\text{Ne}(\beta^+){}^{17}\text{F}$	$\frac{1}{2}^-\frac{3}{2}$	$\frac{3}{2}^-\frac{1}{2}$	3.530 ± 0.000	13.318 ± 0.632	44.670 ± 2.596	-1.026 ± 0.286	-13.324 ± 0.442
	$\frac{1}{2}^-\frac{3}{2}$	$\frac{1}{2}^-\frac{1}{2}$	3.525 ± 0.000	11.261 ± 0.033	3.579 ± 0.120	3.137 ± 0.112	5.838 ± 0.106
${}^{20}\text{F}(\beta^-){}^{20}\text{Ne}; {}^{20}\text{Na}(\beta^+){}^{20}\text{Ne}$	2^+1	2^+0	1.167 ± 0.000	6.169 ± 0.211	14.201 ± 0.636	20.374 ± 0.130	20.164 ± 0.246
${}^{20}\text{O}(\beta^-){}^{20}\text{F}; {}^{20}\text{Mg}(\beta^+){}^{20}\text{Na}$	0^+2	1^+1	0.742 ± 0.000	8.940 ± 0.136	12.402 ± 0.077	-1.071 ± 0.021	-11.096 ± 0.526
${}^{21}\text{F}(\beta^-){}^{21}\text{Ne}; {}^{21}\text{Mg}(\beta^+){}^{21}\text{Na}$	$\frac{5}{2}^+\frac{3}{2}$	$\frac{3}{2}^+\frac{1}{2}$	2.341 ± 0.000	5.879 ± 0.122	10.650 ± 0.610	18.342 ± 0.206	22.311 ± 0.412
	$\frac{5}{2}^+\frac{3}{2}$	$\frac{5}{2}^+\frac{1}{2}$	0.131 ± 0.000	6.145 ± 0.025	11.068 ± 0.045	-256.639 ± 0.349	-417.041 ± 0.652
${}^{22}\text{O}(\beta^-){}^{22}\text{F}; {}^{22}\text{Si}(\beta^+){}^{22}\text{Al}$	0^+3	1^+2	7.665 ± 0.000	96.917 ± 0.283	88.616 ± 0.135	79.224 ± 0.158	87.694 ± 0.050
${}^{24}\text{Ne}(\beta^-){}^{24}\text{Na}; {}^{24}\text{Si}(\beta^+){}^{24}\text{Al}$	0^+2	1^+1	1.725 ± 0.000	0.958 ± 0.428	21.225 ± 0.497	0.860 ± 0.020	14.754 ± 0.033
${}^{25}\text{Na}(\beta^-){}^{25}\text{Mg}; {}^{25}\text{Si}(\beta^+){}^{25}\text{Al}$	$\frac{5}{2}^+\frac{3}{2}$	$\frac{5}{2}^+\frac{1}{2}$	0.334 ± 0.460	1.958 ± 0.717	3.072 ± 2.535	9.610 ± 0.428	6.632 ± 0.181
	$\frac{5}{2}^+\frac{3}{2}$	$\frac{3}{2}^+\frac{1}{2}$	0.956 ± 0.000	-0.523 ± 0.013	9.335 ± 0.082	0.396 ± 0.011	0.239 ± 0.207
${}^{26}\text{Na}(\beta^-){}^{26}\text{Mg}; {}^{26}\text{P}(\beta^+){}^{26}\text{Si}$	3^+2	2^+1	0.079 ± 0.023	4.278 ± 0.159	13.040 ± 1.958	-50.555 ± 1.185	61.994 ± 2.848
${}^{31}\text{Al}(\beta^-){}^{31}\text{Si}; {}^{31}\text{Ar}(\beta^+){}^{31}\text{Cl}$	$\frac{5}{2}^+\frac{5}{2}$	$\frac{3}{2}^+\frac{3}{2}$	1.336 ± 1.543	-1.518 ± 0.251	9.089 ± 2.899	-9.307 ± 1.248	-7.650 ± 0.624

TABLE III. Experimental data for $\log ft$ [34]. The + (-) label indicates the β^+ (β^-) decays. The 0 (1) label indicates the lower (upper) admixed states.

Mirror Pair	$J_i^\pi T_i$	$J_f^\pi T_f$	$\log ft^{0-}$	$\log ft^{1-}$	$\log ft^{0+}$	$\log ft^{1+}$
${}^8\text{Li}(\beta^-){}^8\text{Be}; {}^8\text{B}(\beta^+){}^8\text{Be}$	2^+1	2^+0	5.589 ± 0.008		5.622 ± 0.008	3.01 ± 0.05
${}^{12}\text{B}(\beta^-){}^{12}\text{C}; {}^{12}\text{N}(\beta^+){}^{12}\text{C}$	1^+1	0^+0	4.0617 ± 0.0005	4.572 ± 0.017	4.1106 ± 0.0007	4.622 ± 0.01
${}^{13}\text{B}(\beta^-){}^{13}\text{C}; {}^{13}\text{O}(\beta^+){}^{13}\text{N}$	$\frac{3}{2}^-\frac{3}{2}$	$\frac{1}{2}^-\frac{1}{2}$	4.034 ± 0.006	4.59 ± 0.09	4.081 ± 0.011	4.66 ± 0.1
	$\frac{3}{2}^-\frac{3}{2}$	$\frac{3}{2}^-\frac{1}{2}$	4.45 ± 0.05	4.95 ± 0.2	4.55 ± 0.01	5.09 ± 0.15
${}^{17}\text{N}(\beta^-){}^{17}\text{O}; {}^{17}\text{Ne}(\beta^+){}^{17}\text{F}$	$\frac{1}{2}^-\frac{3}{2}$	$\frac{3}{2}^-\frac{1}{2}$	4.416 ± 0.015	3.851 ± 0.013	4.65 ± 0.03	3.895 ± 0.024
	$\frac{1}{2}^-\frac{3}{2}$	$\frac{1}{2}^-\frac{1}{2}$	7.08 ± 0.09	4.37 ± 0.04	7.13 ± 0.19	4.55 ± 0.02
${}^{20}\text{F}(\beta^-){}^{20}\text{Ne}; {}^{20}\text{Na}(\beta^+){}^{20}\text{Ne}$	2^+1	2^+0	4.9788 ± 0.0003		4.987 ± 0.003	4.196 ± 0.007
${}^{20}\text{O}(\beta^-){}^{20}\text{F}$	0^+2	1^+1	3.734 ± 0.0006	3.64 ± 0.06	3.81 ± 0.03	4.06 ± 0.07
${}^{21}\text{F}(\beta^-){}^{21}\text{Ne}; {}^{21}\text{Mg}(\beta^+){}^{21}\text{Na}$	$\frac{5}{2}^+\frac{3}{2}$	$\frac{3}{2}^+\frac{1}{2}$	5.67 ± 0.14	4.52 ± 0.03	5.26 ± 0.13	4.48 ± 0.03
	$\frac{5}{2}^+\frac{3}{2}$	$\frac{5}{2}^+\frac{1}{2}$	4.662 ± 0.002	7.1 ± 0.6	7.72 ± 0.27	5.9 ± 0.17
${}^{22}\text{O}(\beta^-){}^{22}\text{F}; {}^{22}\text{Si}(\beta^+){}^{22}\text{Al}$	0^+3	1^+2	4.6 ± 0.1	3.8 ± 0.1	5.09 ± 0.09	3.83 ± 0.05
${}^{24}\text{Ne}(\beta^-){}^{24}\text{Na}; {}^{24}\text{Si}(\beta^+){}^{24}\text{Al}$	0^+2	1^+1	4.364 ± 0.003	4.4 ± 0.012	4.36 ± 0.05	4.45 ± 0.03
${}^{25}\text{Na}(\beta^-){}^{25}\text{Mg}; {}^{25}\text{Si}(\beta^+){}^{25}\text{Al}$	$\frac{5}{2}^+\frac{3}{2}$	$\frac{5}{2}^+\frac{1}{2}$	5.25 ± 0.02	6.04 ± 0.1	5.24 ± 0.14	6.21 ± 0.13
	$\frac{5}{2}^+\frac{3}{2}$	$\frac{3}{2}^+\frac{1}{2}$	5.05 ± 0.03	5.19 ± 0.08	5.05 ± 0.08	5.43 ± 0.03
${}^{26}\text{Na}(\beta^-){}^{26}\text{Mg}; {}^{26}\text{P}(\beta^+){}^{26}\text{Si}$	3^+2	2^+1	4.71 ± 0.01	7.6 ± 0.4	4.9 ± 0.1	5.9 ± 0.3
${}^{31}\text{Al}(\beta^-){}^{31}\text{Si}; {}^{31}\text{Ar}(\beta^+){}^{31}\text{Cl}$	$\frac{5}{2}^+\frac{5}{2}$	$\frac{3}{2}^+\frac{3}{2}$	4.77 ± 0.06	4.47 ± 0.13	4.93 ± 0.02	4.55 ± 0.06

TABLE IV. Numerical results for the residuals defined in Eq. (2), (10), and (12). The + (-) label indicates the β^+ (β^-) decays. The 0 (1) label indicates the lower (upper) admixed states.

Mirror pairs	$J_i^\pi T_i$	$J_f^\pi T_f$	Δ_I^0	Δ_I^1	Δ_{II}^+	Δ_{II}^-	Δ_{III}
${}^8\text{Li}(\beta^-){}^8\text{Be}; {}^8\text{B}(\beta^+){}^8\text{Be}$	2^+1	2^+0	-0.075 ± 0.036		-350.048 ± 29.453		
${}^{12}\text{B}(\beta^-){}^{12}\text{C}; {}^{12}\text{N}(\beta^+){}^{12}\text{C}$	1^+1	0^+0	-0.046 ± 0.011	0.097 ± 0.025	3.440 ± 0.285	3.396 ± 0.285	0.193 ± 0.018
${}^{13}\text{B}(\beta^-){}^{13}\text{C}; {}^{13}\text{O}(\beta^+){}^{13}\text{N}$	$\frac{3}{2}^-\frac{3}{2}$	$\frac{1}{2}^-\frac{1}{2}$	0.040 ± 0.017	0.140 ± 0.158	-0.168 ± 0.320	-0.194 ± 0.320	0.164 ± 0.108
	$\frac{3}{2}^-\frac{3}{2}$	$\frac{3}{2}^-\frac{1}{2}$	0.123 ± 0.066	0.294 ± 0.345	4.139 ± 0.005	4.096 ± 0.016	0.319 ± 0.175
${}^{17}\text{N}(\beta^-){}^{17}\text{O}; {}^{17}\text{Ne}(\beta^+){}^{17}\text{F}$	$\frac{1}{2}^-\frac{3}{2}$	$\frac{3}{2}^-\frac{1}{2}$	0.400 ± 0.063	0.230 ± 0.031	10.070 ± 0.166	9.314 ± 0.054	-0.164 ± 25.412
	$\frac{1}{2}^-\frac{3}{2}$	$\frac{1}{2}^-\frac{1}{2}$	0.199 ± 0.236	0.487 ± 0.068	-376.352 ± 73.871	-458.765 ± 42.412	0.299 ± 0.285
${}^{20}\text{F}(\beta^-){}^{20}\text{Ne}; {}^{20}\text{Na}(\beta^+){}^{20}\text{Ne}$	2^+1	2^+0	-0.061 ± 0.007		-5.188 ± 0.046		
${}^{20}\text{O}(\beta^-){}^{20}\text{F}; {}^{20}\text{Mg}(\beta^+){}^{20}\text{Na}$	0^+2	1^+1	0.157 ± 0.036	1.731 ± 0.243	0.121 ± 0.013	-0.566 ± 0.002	1.142 ± 0.168
${}^{21}\text{F}(\beta^-){}^{21}\text{Ne}; {}^{21}\text{Mg}(\beta^+){}^{21}\text{Na}$	$\frac{5}{2}^+\frac{3}{2}$	$\frac{3}{2}^+\frac{1}{2}$	-0.659 ± 0.075	-0.128 ± 0.039	-1.249 ± 0.876	-10.407 ± 2.224	1.432 ± 0.453
	$\frac{5}{2}^+\frac{3}{2}$	$\frac{5}{2}^+\frac{1}{2}$	$1,141.829\pm 308.586$	0.667 ± 0.040	216.797 ± 58.532	0.023 ± 0.000	-2.555 ± 0.007
${}^{22}\text{O}(\beta^-){}^{22}\text{F}; {}^{22}\text{Si}(\beta^+){}^{22}\text{Al}$	0^+3	1^+2	2.173 ± 0.416	-0.013 ± 0.120	40.728 ± 1.623	53.564 ± 0.520	$-0.652\pm 48,769.831$
${}^{24}\text{Ne}(\beta^-){}^{24}\text{Na}; {}^{24}\text{Si}(\beta^+){}^{24}\text{Al}$	0^+2	1^+1	-0.212 ± 0.050	-0.017 ± 0.036	2.216 ± 0.038	2.057 ± 0.005	0.474 ± 0.067
${}^{25}\text{Na}(\beta^-){}^{25}\text{Mg}; {}^{25}\text{Si}(\beta^+){}^{25}\text{Al}$	$\frac{5}{2}^+\frac{3}{2}$	$\frac{5}{2}^+\frac{1}{2}$	-0.034 ± 0.141	0.509 ± 0.243	0.000 ± 0.308	-0.063 ± 0.307	0.495 ± 0.292
	$\frac{5}{2}^+\frac{3}{2}$	$\frac{3}{2}^+\frac{1}{2}$	-0.099 ± 0.085	0.739 ± 0.148	0.534 ± 0.030	0.182 ± 0.022	0.835 ± 7.415
${}^{26}\text{Na}(\beta^-){}^{26}\text{Mg}; {}^{26}\text{P}(\beta^+){}^{26}\text{Si}$	3^+2	2^+1	0.461 ± 0.157	-2.106 ± 0.032	-0.143 ± 0.016	0.006 ± 0.004	0.226 ± 0.037
${}^{31}\text{Al}(\beta^-){}^{31}\text{Si}; {}^{31}\text{Ar}(\beta^+){}^{31}\text{Cl}$	$\frac{5}{2}^+\frac{5}{2}$	$\frac{3}{2}^+\frac{3}{2}$	0.339 ± 0.096	0.186 ± 0.173	-0.212 ± 4.124	-0.055 ± 4.125	$-0.046\pm 10,047.546$